C. R. Physique 16 (2015) 356–367

Contents lists available at ScienceDirect

Comptes Rendus Physique

www.sciencedirect.com

Highlights of the LHC run 1 / Résultats marquants de la première période d'exploitation du GCH

The ATLAS and CMS detectors at the LHC

Les détecteurs ATLAS et CMS auprès du LHC

Daniel Fournier [a,*], Tejinder Virdee [b]

[a] *LAL, Université Paris-Sud, CNRS/IN2P3, Orsay, France*
[b] *Imperial College, University of London, London, United Kingdom*

ARTICLE INFO

Article history:
Available online 14 May 2015

Keywords:
Calorimeter
Spectrometer
Solenoid
Toroid
Higgs boson
Top quark

Mots-clés :
Calorimètre
Spectromètre
Solenoide
Toroide
Boson de Higgs
Quark top

ABSTRACT

The construction of the LHC detectors presented formidable challenges and, together with physics exploitation, has required the resources and talents of many thousands of scientists and engineers.

© 2015 Académie des sciences. Published by Elsevier Masson SAS. All rights reserved.

RÉSUMÉ

La construction des détecteurs auprès du LHC représentait un formidable défi et, en même temps que l'exploitation de la physique, elle a requis les compétences de plusieurs milliers de scientifiques et ingénieurs talentueux.

© 2015 Académie des sciences. Published by Elsevier Masson SAS. All rights reserved.

1. Design requirements

At the design energy of the LHC, 14 TeV in the centre of mass, the production cross-section of "new physics" is small, e.g., less than 100 pb for the long-sought Standard Model (SM) Higgs boson, while the inelastic proton–proton cross-section is close to 100 mb (see Fig. 1). Taking into account that only some rather rare decay modes with a clean signature could lead to a large enough signal to background ratio, an instantaneous luminosity of 10^{34} cm^{-2} s^{-1} was the target to be met in order to "guarantee" the discovery at the LHC of the SM Higgs boson, its mass being limited by several theoretical arguments to $\simeq$1 TeV.

The above two key numbers for energy and luminosity set the scale of the challenges to be met by the detectors: at this luminosity, and with proton bunches colliding every 25 ns, one expects an average of 20 inelastic collisions per bunch crossing (bc). These additional interactions in general produce only rather soft particles (mostly pions) and create what is called the pile-up noise. If the sensitive time of the detectors is longer than 25 ns, several bc are added up, meaning an effective increase of the pile-up. Therefore the detectors' response has to be fast, of the order of 25 ns, especially for those detectors where the particle density is highest, close to the collision point. With an average multiplicity of about six

* Corresponding author.
E-mail address: daniel.fournier@cern.ch (D. Fournier).

http://dx.doi.org/10.1016/j.crhy.2015.03.018
1631-0705/© 2015 Académie des sciences. Published by Elsevier Masson SAS. All rights reserved.

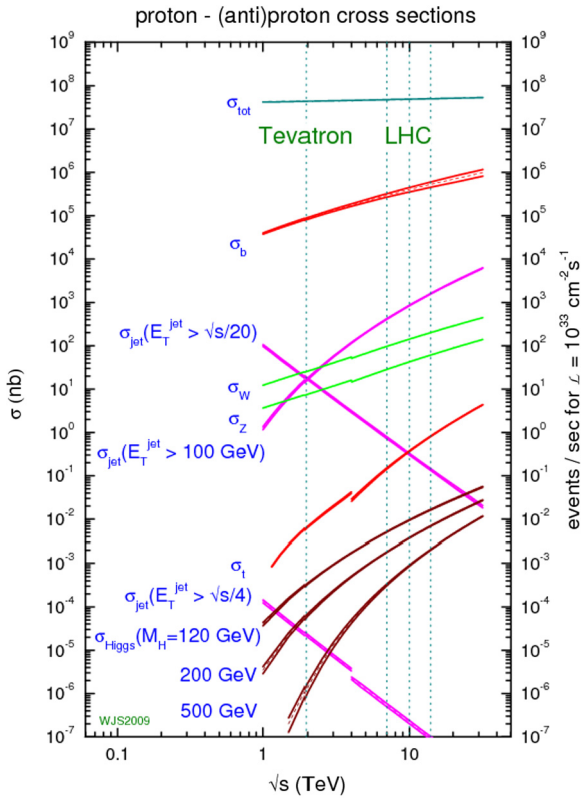

Fig. 1. (Color online.) Cross-sections for important physics processes as a function of centre of mass energy. Below 3 TeV, the cross-sections correspond to a $p\bar{p}$ initial state, as was the case for the Tevatron near Chicago (maximum energy of 2 TeV in the centre of mass).

charged particles per pseudo-rapidity[1] unit, each with an average transverse momentum of $\simeq 0.5$ GeV, and an almost equal number of photons, the soft collisions creating the pile-up noise also lead to energy deposition in the detectors, giving rise to a sizeable (ionising and non-ionising) radiation fluence. Radiation resistance was a rather new, and difficult, challenge to be met by detectors, sensors and "on-detector" electronics.

During "run I", i.e. the data taking period from 2010 to 2012, the energy was actually limited to 8 TeV (7 TeV in 2010 and 2011), and the collisions took place every 50 ns. This resulted in a maximum instantaneous luminosity of about $0.8 \cdot 10^{34}$ cm^{-2} s^{-1}, with an average number of inelastic collisions per bc of 20.7, i.e. the nominal value, and up to 40 in some cases.

1.1. General features

The LHC detectors feature a tracking and vertexing system around the collision point, immersed in a strong magnetic field, surrounded by an electromagnetic calorimeter optimised for the identification and accurate measurement of the energy of electrons and photons, which is itself surrounded by the hadronic calorimeter. The two calorimeters together contain and measure the energies of jets resulting from the materialisation of quarks and gluons. Muons are the only charged particles able to traverse the calorimeters (where they lose about 3 GeV). They are identified in the muon spectrometer behind, and measured both inside the tracker and in the spectrometer. The production of escaping particles such as neutrinos is deduced from a significant imbalance in the visible momenta of the detected particles in the plane transverse to the beam direction. See Fig. 2 for illustration.

The transverse momentum (p_T) measurement of charged particles in the tracking volume, and/or in the muon spectrometer derives from the sagitta of the corresponding curved tracks. The choice of the magnetic system to a large extent determines the geometry of the experiment. CMS uses a classical solenoid geometry, however of unprecedented size and field. ATLAS also uses a small solenoid for the tracking volume, but the choice was made to have in addition a separate large toroidal system around the calorimeters, specific to the muon spectrometer. The parameters of both magnet systems were dictated by the requirement of measuring muon p_T to better than 10% at 1 TeV, in view of understanding the behaviour of a possible Z′ (heavy partners of the Z in extended models) up to an invariant mass of a few TeV. An illustration is given in Section 2.1.

[1] Pseudorapidity is defined as $\eta = -\ln\tan\frac{\theta}{2}$ in terms of the polar angle θ measured from the z axis along the anticlockwise beam direction.

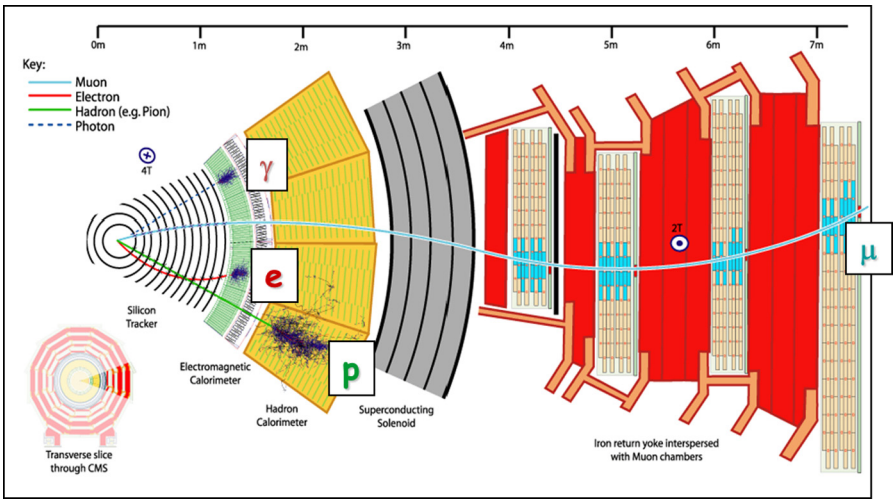

Fig. 2. (Color online.) Slice of a LHC detector (example of CMS) as a "Russian doll", with an illustration of the main functions.

1.2. Calorimetry

The decay modes of the SM Higgs boson change drastically as a function of its mass (see "Higgs" Chapter). Already in the 1990s, it was clear that the region around 130 GeV, not excluded by precision electroweak data, would be particularly difficult to cover. The most promising mode in this mass range is the diphoton mode (coupling generated by top and W loops). This mode became the benchmark to evaluate candidate devices for electromagnetic calorimetry. There was no candidate technology meeting at the same time the requirements on high resolution (to clearly observe a small signal on a large background), high granularity (to reject the background from jets, larger by a factor of about 10^6 than the irreducible diphoton background), high speed (to limit pile-up), and radiation resistant (to ensure stable response irrespective of the variation of luminosity during data taking, and sufficient lifetime).

Several R&D programmes were launched, particularly on scintillating inorganic crystals (in view of improving their radiation resistance) and on noble liquids, working as ionisation detectors (in view of improving their speed and granularity). The successful outcomes are the $PbWO_4$ crystal calorimeter of CMS and the "accordion" liquid argon calorimeter of ATLAS. Beside the detectors themselves, a further challenge was the design of front-end electronics that had to have low-power consumption, to be radiation resistant, and capable of covering a dynamic range from a few tens of MeV (level of the electronics noise) to several TeV (energy of the largest anticipated signals, for example from a Z' decaying in an electron–positron pair).

With less challenging requirements on granularity and resolution, the hadronic calorimeters are comparatively easier. To fit a deep enough (10 interaction lengths) hadronic calorimeter in the CMS solenoid was however a challenge. In the forward direction, the requirement of as accurate as possible missing transverse energy measurement called for coverage up to a pseudo rapidity $|\eta| = 5$, where the high radiation level is a challenge. This was achieved with liquid argon in ATLAS, and with an iron-quartz fiber device, recessed to 11 m from the collision point, in CMS.

As opposed to momentum measurements in magnetic field, the relative resolution of calorimeters improves with energy, typically as its square root. There are however limitations (described by the so-called "constant term") related to uniformity, stability with time and accuracy of the calibration. In practice, for large systems, it is challenging to reach accuracies significantly below 1%, even for the most performant electromagnetic calorimeters.

1.3. Tracking and vertexing

Powerful tracking and vertexing (tracking close to the vertex) are among the most important requirements of any colliding beam experiment, and the LHC experiments are no exception in this respect. The first requirement is the efficient reconstruction of up to about 50 vertices present in a single bc. The rms of their longitudinal position, determined by the longitudinal size of the proton bunches is about 6 cm, while transversally the typical spread is about 20 μm. This is illustrated by Fig. 3. The other main requirement, equally important, is the capability of finding secondary vertices corresponding to the decays of particles with short lifetimes (about 1.5 ps in the case of b-hadrons, about 0.3 ps in the case of taus), or at least to sign the presence of such decays by finding the tracks that do not come exactly from the collision vertex, and have a positive impact parameter. The scale is set by the typical impact parameter of a particle from the decay of a "parent" particle with a lifetime of 1.5 ps, which is typically 450 μm.

The choice detectors for vertexing are silicon sensors (with pixel or microstrip cells). They give rise to fast signals, are rather thin (typically 250 μm), operated at moderate voltage, and do not require an operating gas. With thin strip patterns, they have already been abundantly used, with excellent results, most recently at the Tevatron. With the many vertices per bunch crossing at the LHC, and the rather high multiplicity of hard collisions, strip patterns would lead to too many

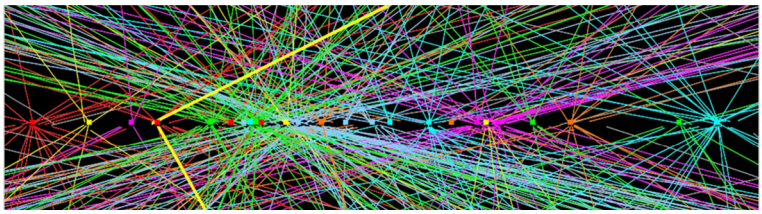

Fig. 3. (Color online.) An example of the reconstructed position of interaction vertices at a luminosity of $0.7 \cdot 10^{33}$ cm^{-2} s^{-1}. The tracks in yellow correspond to the two muons, identified in the muon spectrometer, of a $Z \to \mu\mu$ candidate.

ambiguities. The solution is to go to elementary pixels, of typically 50 μm in rϕ and 400 μm along the beam line. With such a checkerboard pattern, it is straightforward to calculate that a three-layer pixel system, arranged as cylinders and complemented by forward disks, covering the whole collision area, would have at least 50 million pixels. Compared to previous devices, this was clearly a new scale, requiring novel developments. In particular with such a density, sensors and electronics chips have to be coupled "face to face" by bump-bonding, a technique developed for this purpose.

The tough requirements above are made even more difficult by the fact that the vertex detectors have to operate in a very harsh radiation environment (typically, at the level of the innermost pixel layer, 0.1 MGy of ionising dose and 10^{14} 1-MeV neutrons equivalent per cm^2 per year at nominal luminosity). On the sensors the most important adverse effects result from non-ionising damage (by neutrons, protons, pions) which create dislocations in the bulk of the silicon crystals. In turn those create deep levels that trap the drifting charges, thus reducing the ionisation signal, and furthermore generate leakage current, which in turn leads to heat dissipation. In general, under irradiation, the base material evolves towards the p type. This is why both experiments used "n-on-n" sensors. To limit the radiation effects, the operating temperature of the vertex detectors is lowered to $-10\,^{\circ}$C or less.

The damage from radiation to electronics can be mitigated to some level by design. In France the DMILL technology was launched for this purpose. It is used for the ATLAS SCT, TRT, and the liquid argon front-end electronics. While some of the first pixel prototypes were designed with this technology, the 250-nm CMOS technology soon appeared superior in terms of yield, and was used for production of many of the chips, including those of ATLAS pixels and CMS silicon tracker and electromagnetic calorimeter. A pixel front-end chip has typically a surface close to 1 cm^2, serving about 3000 pixels, and counts more than one million transistors.

1.4. Event selection

The first signature used to identify interesting "hard processes" (among which is Higgs boson production) is the p_T of the detected objects: either jets signing the materialisation of quarks or gluons, or leptons (electrons, muons and taus), or photons. The vast majority of bc do not contain a high p_T object, and the corresponding information is almost immediately erased from the front-end buffers. The interesting ones, with at least one high p_T object, are submitted to tighter and tighter kinematic constraints such that a global rate of about 500 events per second written to permanent storage is reached, while keeping a very high efficiency for the physics of interest. This is obtained by identifying on line the high p_T objects as leptons or photons, for which a lower threshold is affordable than for jets. When rather low p_T are mandatory, additional objects in coincidence are required. All these possibilities together form the "trigger menu", which is dynamically tuned to the instantaneous luminosity.

The rate of production of jets by strong interactions (Quantum chromodynamics QCD) is so large (see Fig. 1) that p_T thresholds around 100 GeV, or large jet multiplicities are necessary to satisfy the bandwith allocated to pure QCD triggers. On the contrary, leptons (photons) are much less frequent, and the corresponding thresholds for single objects can be lowered to about 30 (50) GeV (provided the jet background rejection is sufficient), for catching final states with vector boson production (W and Z), or Higgs boson production, or more exotic final states. As opposed to electroweak couplings, which are universal between the three flavors of charged leptons, the SM Higgs boson couples to fermions (leptons and quarks) proportionnally to their mass, thus giving a special role to tau leptons, and also to top and bottom quarks. The signature of those final states is thus particularly important. Electrons and photons are identified by the characteristics of the shower they create in the electromagnetic calorimeters (together with the presence of a "matching" track in the case of electrons). Muons are in principle the only charged particles capable of traversing the hadronic calorimeters surrounding the EM one. Tau leptons have several competing decay modes, all including neutrinos (that escape the detector) and their signature is difficult, particularly at the trigger level. Hadrons with b-flavour are identified by selecting jets containing a secondary vertex, or one or more tracks with a significant impact parameter.

2. ATLAS

The main design performances of ATLAS, in terms of measurement precision and coverage, are summarised in Table 1. More details on the design and construction can be found in Ref. [1].

Table 1
Main design performance of the ATLAS experiment (E and P_T in GeV).

Detector component	Required resolution	η coverage	
		Measurement	Trigger
Tracking	$\sigma_{P_T}/P_T = 0.05\%\ P_T \oplus 1\%$	± 2.5	
EM Calorimetry	$\sigma_E/E = 10\%/\sqrt{E} \oplus 0.7\%$	± 3.2	± 2.5
Hadronic calorimetry (jets)			
barrel and end-cap	$\sigma_E/E = 50\%/\sqrt{E} \oplus 3\%$	± 3.2	± 3.2
forward	$\sigma_E/E = 100\%/\sqrt{E} \oplus 10\%$	$3.1 < \|\eta\| < 4.9$	$3.1 < \|\eta\| < 4.9$
Muon spectrometer	$\sigma_{P_T}/P_T = 10\%$ at $P_T = 1$ TeV	± 2.7	± 2.4

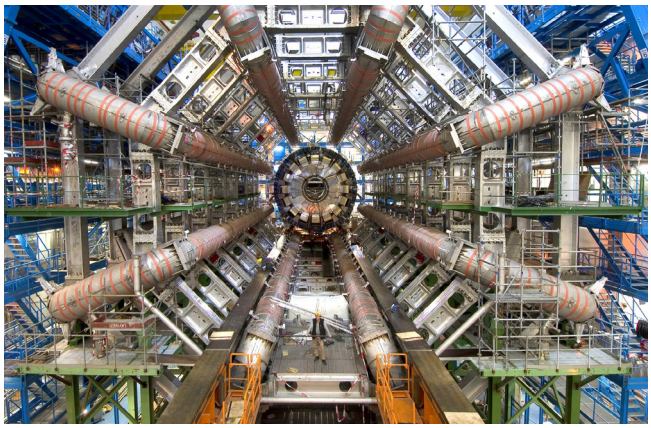

Fig. 4. (Color online.) A photograph of ATLAS during installation, showing the eight coils of the muon spectrometer barrel. Visible in the centre is the barrel calorimeter right before it was longitudinally pushed to the centre of the experiment.

2.1. Muon spectrometer

The muon spectrometer forms the outer part of the ATLAS detector and is designed to detect charged particles exiting the barrel and end-cap calorimeters and to measure their momentum in the pseudorapidity range $|\eta| < 2.7$. It is also designed to trigger on these particles in the region $|\eta| < 2.4$. The magnetic field is provided by one barrel and two end-cap superconducting toroids, each featuring eight coils. In this geometry, the magnetic field lines are closed inside the volume delimited by the coils, and no iron for field return is necessary.

Fig. 4 shows the barrel part installed in the pit. The barrel toroid length is 25 m and its inner (outer) diameter is 9.4 (20.1) m. The operating current is 20 kA, and the average field is typically 0.5 T in the barrel, and 1 T in the end-caps. In this system the sagitta of a 1-TeV muon is typically 0.5 mm. Thus a measurement with a relative precision of 10% requires a single position measurement precision better than 50 µm. This is achieved using multilayers of drift tubes, whose position is determined with a high precision using a laser alignment system, and using the tracks themselves. The trigger system is based on RPCs (resistive plate chambers) in the barrel part, and on TGCs (thin gap proportional chambers) in the end-cap part.

Once a muon candidate is reconstructed in the muon spectrometer, it is extrapolated to the inner detector (ID) volume where a corresponding track should be present. The information from the two segments is combined for an optimum performance, the resolution from the ID being in general better for low p_T, while the spectrometer is better at high p_T. The refined calibration of the momentum scale of muons is made using the precisely known mass of the J/ψ, Υ and Z resonances. The invariant mass resolution of a $Z \to \mu\mu$ candidate is typically 2%. The behaviour at high di-muon invariant mass is illustrated in Fig. 5 where, above the overwhelming Z peak, the agreement between data and simulation spans over six decades. The same is true for the $Z \to ee$ distribution.

2.2. Calorimeters

The ID, its solenoid and the calorimeters are installed inside the space of inner radius $\simeq$4.5 m inside the bore of the barrel toroid. In order to save radial space, the solenoid shares its insulation vacuum with the barrel liquid argon electromagnetic calorimeter. At larger radii, the hadronic calorimeter is made out of a sandwich of scintillator plates and iron—a cost-effective solution given the high total mass of $\simeq$1000 t. The end-cap and forward calorimeters (see Fig. 6) use the liquid argon technique that is largely immune against radiation damage. For better shower containment, tungsten is used

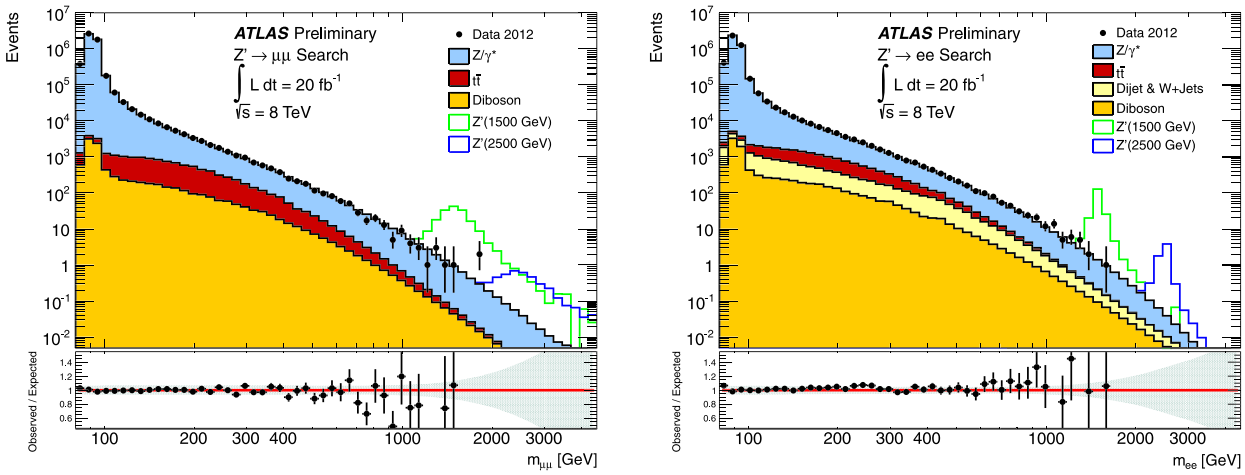

Fig. 5. (Color online.) Invariant mass spectrum of di-muons (left) and di-electrons (right) observed in ATLAS. The simulation of the signals from a Z′ (high mass recurrence of the Z in some exotic models) at 1.5 and 2.5 TeV indicates the expected resolution in each case.

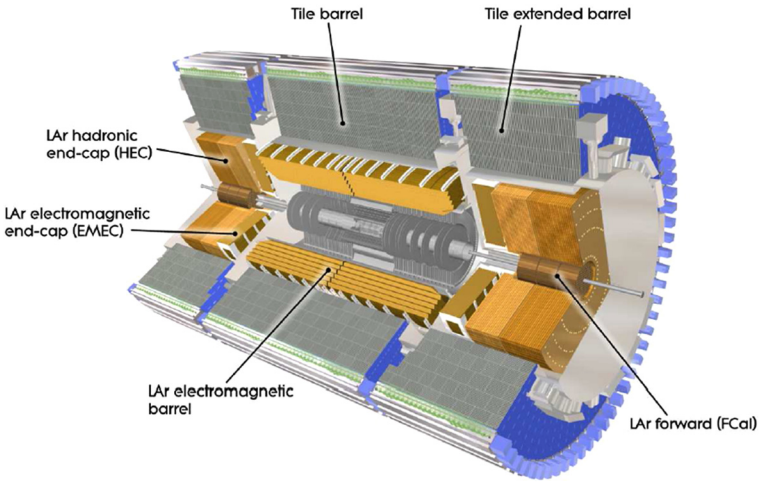

Fig. 6. (Color online.) Electromagnetic and hadronic calorimeters of the ATLAS experiment. The inner detector, with its pixel, SCT and TRT components is visible inside the calorimeter bore.

as a passive material in the most forward part ($|\eta| > 3.2$). With the techniques used, charged pions, which constitute the dominant component of hadronic jets, give rise to signals of a comparatively smaller size, for the same energy, than those of electrons and photons. Taking advantage of the high granularity, this effect is mitigated to some extent by pattern recognition and dedicated calibration of the two components. In this way, a satisfactory linearity is obtained, up to the highest relevant energies ($\simeq$3 TeV).

The liquid-argon electromagnetic calorimeter uses the "accordion geometry" (see Fig. 7), which allows high granularity while preserving the fast rise time of signals. The granularity in $\Delta\eta \times \Delta\phi$ is 0.003×0.1 for the first sampling, 0.025×0.025 for the second one and 0.05×0.025 for the last one. The calorimeter is preceded in the cryostat by a presampler that enables a correction to be applied for energy lost in upstream material (ID, cryostat, solenoid). In total there are close to 200 000 readout channels. The front-end electronics uses the derivative of the current signal (see Fig. 7), providing a signal with a rise time of $\simeq$40 ns and a total duration of $\simeq$100 ns adequate for calorimetry. The dynamic range is covered using three gain ranges and a 12-bit digitisation for each one. The liquid bath is operated at a pressure of 1.25 bar (absolute), and a temperature of 87 K. The purity of the liquid and its temperature stability were such that no correction was necessary for data sets taken over periods of several months.

The large sample (five millions) of $Z \to ee$ reconstructed decays (see Fig. 5) allows to fix the energy scale of electrons (and photons) by reference to the Z mass, and to assess non-uniformities. The performance can be summarised by a constant term slightly below 1% for most of the η range, increasing to less than 2% in some end-cap parts, where the material in front of the calorimeter has some local maxima. The average value of the reconstructed Z mass is found independent of the number of reconstructed vertices (i.e. independent from pile-up) in the whole range observed. Taking the $H \to \gamma\gamma$ channel as a benchmark, its observed invariant mass resolution is about 1.3%. With efficiencies for electrons and photons of 80% or

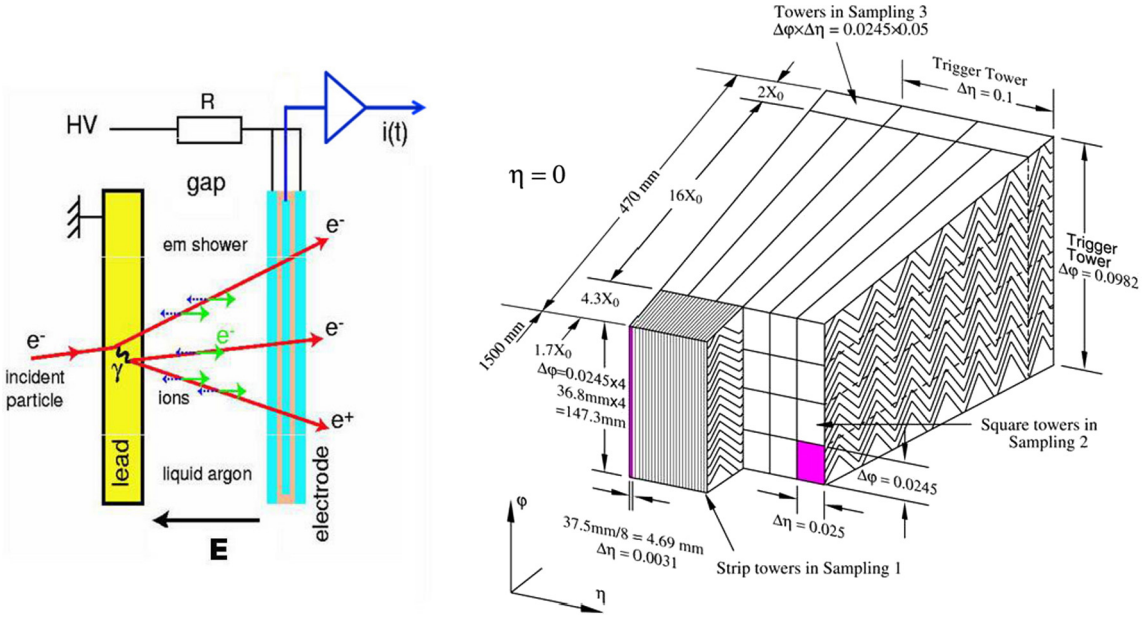

Fig. 7. (Color online.) Illustration of shower development and ionisation collection (left), and sketch of the "accordion" geometry (right) in the ATLAS liquid-argon electromagnetic calorimeter.

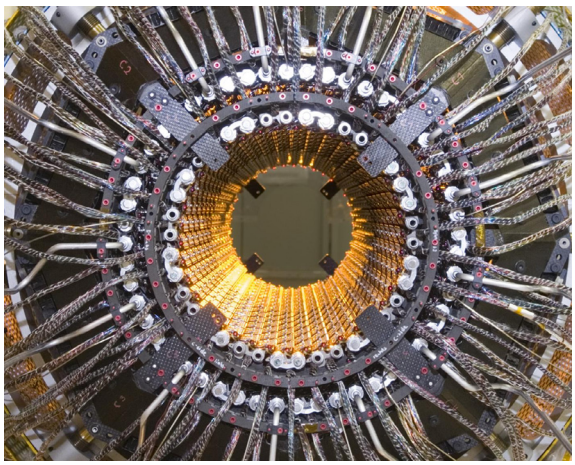

Fig. 8. (Color online.) Photograph of the second cylinder of the ATLAS pixel system during integration. The sensor tilt is well visible, as are the pipes for cooling.

more, in the momentum range of interest ($p_T > 20$ GeV), the rejection of jets faking electromagnetic objects is such that in general the associated backgrounds fall well below irreducible backgrounds from physics origin (see Higgs Chapter for details).

2.3. Inner detector

The main elements of the ID are visible in Fig. 6. The pixel system surrounds the beam pipe (3.6-cm radius) up to a radius, R, of 25 cm where the SCT (silicon strips system) takes over, up to $R = 55$ cm. The largest radius part is occupied by the TRT (transition radiation tracker). The same structure is deployed longitudinally, with disks replacing cylinders.

The pixel sensors are made out of 250-µm-thick detectors, using oxygenated n-type wafers with readout pixels on the n+ implanted side of the detector. This allows a good detection efficiency, even with partial depletion after silicon type inversion. Each sensor has an area of about 64×24 mm, and is equipped with 16 front-end chips, thinned to 180 µm, each serving 2880 pixels of 50×400 µm, for a total of 80 million channels. In the barrel the sensors are slightly tilted (to take into account the Lorentz angle), such that they overlap in $r\phi$. This is visible in Fig. 8, where the cooling pipes for operation at $-10\,^{\circ}$C are also visible. Every effort was made to limit the average material thickness of the pixel system, which is however 0.12 (0.5) radiation lengths at $\eta = 0$ ($\eta = 2$).

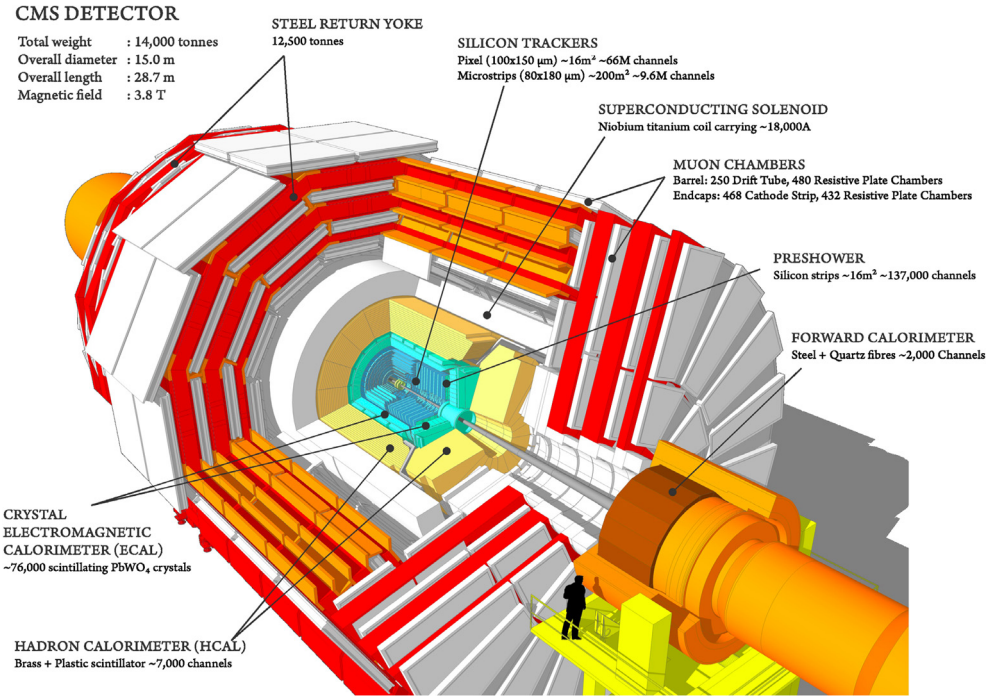

Fig. 9. (Color online.) The layout of the CMS detector.

The SCT system consists of four cylinders of small angle (40 mr) stereo modules, each featuring thin strips with a pitch of 80 μm and a length of about 6 cm. The number of readout channels is 6.3 millions.

The barrel TRT consists of 40 layers of thin polyimide straws (4 mm diameter) with 30-μm-diameter central wires. Polypropylene layers in between straw layers generate X-rays from transition radiation when they are traversed by particle of high Lorentz factor γ, in particular electrons. The straws are operated with Xe–CO_2 gas, in proportional mode. They are sensitive to both ionisation and X-ray conversion into Xe. The electronics (350 000 channels) features a dual threshold discriminator that allows the separation of ionisation signals from those of X-rays. The latter are used as a last additional condition when high-purity electron samples are required. In the end-caps, the straws are positioned as the spokes of the wheels. Given the comparatively large size of straw tubes as compared to silicon strips, the occupancy (number of particles crossing a detector element during one bc) in this detector is higher, up to 30% at high pile-up. However, given the high radial density of straws, the pattern recognition remains efficient, even for the highest pile-up.

The accuracy of space points is 10×115 μm in the pixels, 20×600 μm in the SCT, and about 130 μm in the TRT (one dimension only); in the latter case, the equivalent accuracy is actually better ($\simeq 80$ μm), given the high number of points. Particularly critical for such a precision system is the alignment, whose final steps are based on particle tracks, from cosmic rays and from collisions.

At a p_T of 20 GeV, the accuracy of the impact parameter measurement in rϕ is typically 10 μm.

3. The Compact Muon Solenoid (CMS)

The overall layout of CMS is shown in Fig. 9. The main design performance parameters are summarised in Table 2. More details on the design and construction can be found in Ref. [2]. At the heart of CMS sits a 13-m-long, 5.9-m-diameter, 4-T superconducting solenoid. The return field is large enough to saturate 1.5 m of iron, which accommodates four muon-stations to ensure robustness and full geometric coverage. Each muon station consists of several layers of aluminium drift tubes (DT) in the barrel region and cathode strip chambers (CSC) in the end-cap region, both complemented by resistive plate chambers (RPC). The large diameter and the high field allow a good momentum resolution to be attained without making too stringent demands on muon-chamber resolution and alignment.

The bore of the magnet coil is also large enough to accommodate the inner tracker and the calorimetry inside. The tracking volume is given by a cylinder of 6-m length and 2.6-m diameter. In order to deal with high-track multiplicities, CMS employs ten layers of silicon microstrip detectors that provide the necessary granularity and precision. Silicon pixel detectors placed close to the interaction region improve the measurement of the impact parameter of charged-particle tracks as well as the position of secondary vertices and charged track reconstruction. The electromagnetic calorimeter (ECAL) uses lead tungstate ($PbWO_4$) crystals. The scintillation light is detected by novel Si avalanche photodiodes (APD) in the barrel region and vacuum phototriodes (VPT) in the end-cap region. A silicon-strip-based preshower system is installed in front

Table 2
Main design performance of the CMS experiment (E and p_T in GeV).

Detector component	Required resolution	η coverage	
		Measurement	Trigger
Tracking	$\sigma_{P_T}/P_T = 0.015\%\ P_T \oplus 0.7\%$	± 1.5	
	$\sigma_{P_T}/P_T < 0.6\%\ P_T \oplus 0.7\%$	± 2.5	
EM Calorimetry	$\sigma_E/E = 2\text{–}5\%/\sqrt{E} \oplus 0.6\%$	± 3.0	± 3.0
Hadronic calorimetry (jets)			
barrel and end-cap	$\sigma_E/E = 115\%/\sqrt{E} \oplus 5\%$	± 3.0	± 3.0
forward	$\sigma_E/E = 280\%/\sqrt{E} \oplus 10\%$	$3.0 < \lvert\eta\rvert < 5.0$	$3.0 < \lvert\eta\rvert < 5.0$
Muon spectrometer	$\sigma_{P_T}/P_T = 0.007\%\ P_T \oplus 0.8\%$	± 1.4	± 2.4
	$\sigma_P/P = 0.07\%\ P$	$\eta = 2.0$	

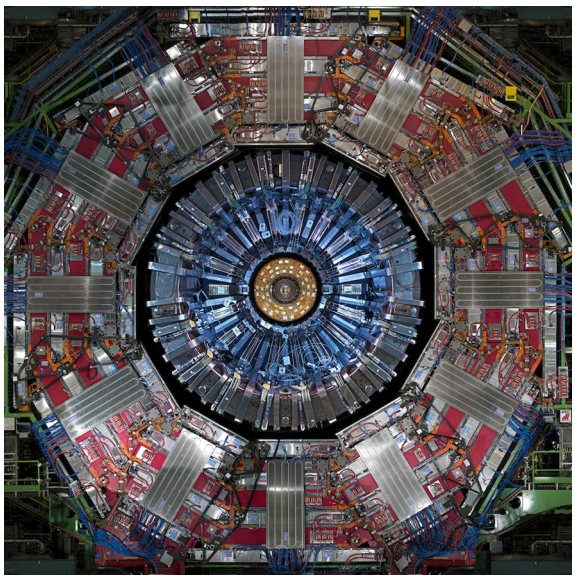

Fig. 10. (Color online.) A photograph of the transverse section of the CMS experiment. The inner tracker, the barrel ECAL and HCAL, the solenoid and the barrel muon system can be seen.

of the endcap ECAL to help with π^0 rejection. The ECAL is surrounded by a brass/scintillator sampling hadron calorimeter. The scintillation light is converted by wavelength shifting (WLS) fibres embedded in the scintillator tiles and channelled to photodetectors via clear fibres. The light is detected by novel photodetectors (Hybrid Photo-Diodes, HPD) that can provide gain and operate in high axial magnetic fields. Coverage up to $|\eta| = 5.0$ is provided by an iron/quartz-fibre calorimeter. The Cerenkov light emitted in the quartz fibres is detected by photomultipliers. The forward calorimeters ensure full geometric coverage ($\eta = 5.0$) for the measurement of the transverse energy in the event.

A photograph of the transverse section of the experiment is shown in Fig. 10. The overall dimensions of the CMS detector are a length of 21.6 m, a diameter of 14.6 mn and a total weight of 14 000 tons.

3.1. Muon spectrometer

Figs. 10 and 11 show the barrel and the endcap parts of the muon system.

In the barrel region ($|\eta| < 1.2$), each one of the four stations contains eight chambers in two groups of four, measuring the muon's coordinate in the r–ϕ bending plane, and four chambers that provide a measurement in the z-direction, along the beam line. The drift cells are offset by a half-cell with respect to their neighbour to eliminate dead areas. Mean-timer circuits are used to determine the time of passage of the candidate muons.

In the end-caps, CSCs cover the region between $0.9 < |\eta| < 2.4$, accounting for overlap with the barrel chambers. Each one of the four stations comprise six chambers, with the cathode strips of each chamber running radially outwards to provide a precision measurement in the r–ϕ bending plane. The anode wires, running approximately perpendicular to the strips, provide measurement in η and the time of passage of the candidate muon.

The RPCs provide an independent, fast and highly granular Level-1 trigger system covering the rapidity range up to $|\eta| = 1.6$. A total of six (three) layers of double-gap RPCs are embedded in the barrel (end-cap) region.

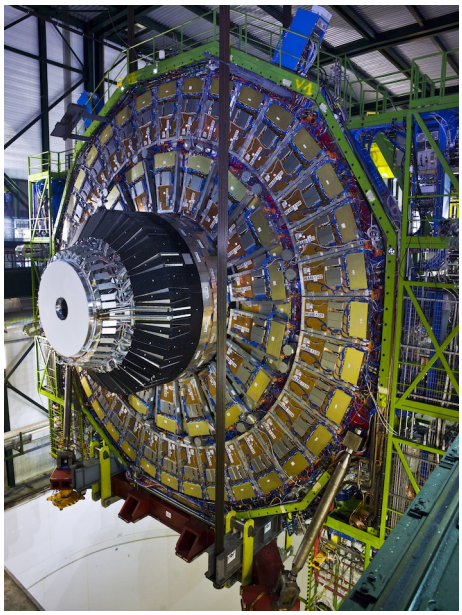

Fig. 11. (Color online.) The steel disk on which the first endcap muon station has been mounted. The CSC chambers can be seen as well as the endcap ECAL and HCAL ("nose").

3.2. The calorimeters

The CMS ECAL is a fine-grained calorimeter comprising 75 848 lead tungstate crystals, arranged in a quasi-projective geometry and distributed in a barrel region ($|\eta| < 1.48$) and two endcaps that extend up to $|\eta| = 3.0$. Lead tungstate is a very dense material, with a short radiation length and Moliere radius. The electromagnetic showers hence are short and very narrow. The lateral granularity ($\Delta\eta \times \Delta\phi \sim 0.017 \times 0.017$ in the barrel region) is high and of the order of the Moliere radius, which is 21 mm, helping in the reconstruction of photons and electrons, especially in an environment of high event pile-up, and for methods of global event reconstruction, sometimes labelled "particle flow" (see below).

The HCAL barrel and end-caps are sampling calorimeters consisting of brass and scintillator plates, covering $|\eta| < 3.0$. The barrel consists of 36 identical azimuthal wedges mounted in two half-barrels. In both the barrel and the end-caps the brass plates, appropriately aligned, are bolted together in a staggered geometry in a configuration that contains no projective dead material over the full radial extent. Gaps of 9 mm are created to insert the active plastic scintillator plates of a thickness of 3.7 mm arranged in a tray (barrel) or petal (endcap) geometry. Source tubes that carry ^{137}Cs radioactive sources are placed such that each tile can be scanned and calibrated. The forward calorimeter (HF), bathed in unprecedented particle fluxes, presented a considerable challenge in terms of radiation hardness of the active material. Quartz fibres were chosen, with a diameter of 600 μm that are inserted in holes created by grooves in diffusion welded iron plates.

3.3. Inner detector

The ID surrounding the interaction region comprises a silicon pixel detector with three barrel layers, situated between 4.4 cm and 10.2 cm, and a silicon microstrip tracker with 10 barrel detection layers extending outwards to a radius of 1.1 m. Two end-caps complete the coverage of the tracker to $|\eta| < 2.5$. It comprises two disks in the pixel detector and 12 disks in the strip tracker on each side of the barrel. The silicon pixel tracker comprises 66 million 100×150 μm^2 pixels. The silicon strip tracker comprises 9.3 million strips with r–ϕ pitch between 80 and 180 μm, with a total silicon surface area of 198 m^2. The inner tracker is designed to operate at a temperature of $-20\,^\circ$C to limit long-term radiation damage.

3.4. Event reconstruction and detector performance

The reconstruction of muon candidates is carried out using two algorithms: the first one, in which the tracks in the silicon detector are matched to segments in the muon chambers, and the second one, in which a combined fit is performed to the signals found in both the silicon tracker and muon systems. The efficiency to reconstruct a muon of $p_T > 5$ GeV is larger than 95%, while the probability to misidentify a hadron as a muon is below 0.1%. For $p_T > 200$ GeV, the precision of the momentum measurement improves when the silicon tracker signals are complemented with the information from the muon chambers. In the barrel region, using through going cosmic rays, the momentum resolution is measured to be $\sigma(p_T)/p_T \sim 7\%$ at $p_T = 1$ TeV.

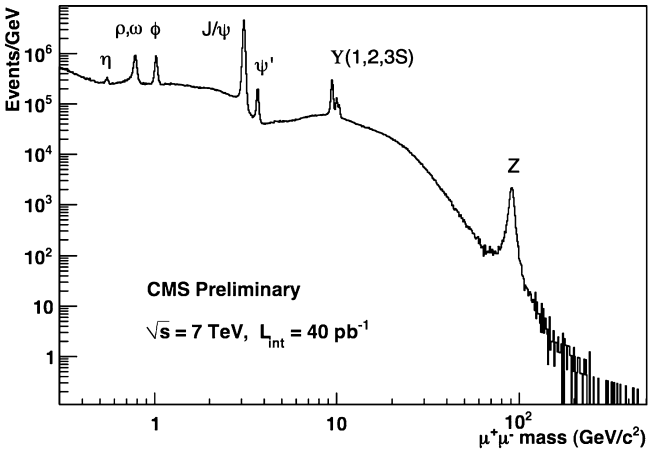

Fig. 12. The distribution of di-muon effective masses showing the various resonant states. The mass resolutions in the central region are: 28 MeV/c^2 (0.9%) for J/ψ, 69 MeV/c^2 (0.7%) for Υ(1S), both dominated by instrumental resolution and $\Gamma = 2.5$ GeV/c^2 for the Z dominated by its natural width.

The energy deposited in the crystals is clustered with algorithms that constrain the clusters in η and ϕ to the shapes expected from electrons and photons with high p_T. Electrons from $Z \to ee$ events provide a measurement of the electron/photon trigger, reconstruction, and identification efficiencies, as well as of the electron/photon energy scale and resolution. For the reconstruction of electrons, the trajectory in the silicon tracker is combined with the clusters in the ECAL taking account of energy loss by bremsstrahlung in the material of the inner tracker and fitted with a Gaussian sum filter. The electron momentum is therefore determined from the combination of ECAL and tracker measurements.

The track-finding efficiency in the inner tracker is larger than 99% for muons with transverse momentum p_T greater than 1 GeV and a transverse momentum resolution between 1.5 and 2.5% for charged tracks of $p_T \sim 100$ GeV in the central region ($|\eta| < 1.5$). Measurements of the impact parameters of charged tracks and secondary vertices are used to identify jets that are likely to contain the hadronisation and decay products of b quarks ("b jets"). A b-jet tagging efficiency of more than 50% is achieved with a rejection factor for light-quark jets of ~200, as measured in $t\bar{t}$ events in data.

CMS uses a "particle-flow" event description algorithm to reconstruct and identify each single particle with an optimised combination of all subdetector information. In this process, the identification of the particle (photon, electron, muon, charged hadron, neutral hadron) plays an important role in the determination of the particle momentum. The reconstructed particles are referred to as objects. Jets are reconstructed by clustering the particle–flow objects with the anti-k_T algorithm using a distance parameter of 0.5. Energy from overlapping pp interactions (pile-up) and from the underlying event is subtracted, e.g., using a technique that is based on the calculation of the η-dependent transverse momentum density, evaluated on an event-by-event basis. The jet momentum is determined as the vector sum of all particle momenta in the jet. Jet energy corrections are derived from simulation studies and from in situ measurements using the energy balance of dijet and $Z/\gamma +$ jet events. The jet momentum resolution achieved is $\sigma(p_T)/p_T = 85\%/\sqrt{p_T}/\text{GeV} \oplus 4\%$ for central jets. The missing transverse energy vector is taken as the negative vector sum of all particle transverse momenta, and its magnitude is referred to as ET_{miss}. The typical missing transverse energy resolution is around $0.5\sqrt{E_T}$ GeV.

The performance of the CMS detector is illustrated in Figs. 12 and 13.

Fig. 12 shows the distribution of invariant masses of all di-muon pairs detected in CMS upon examination of the first three trillion proton–proton interactions. The sharpness of the peaks, corresponding to the labelled particle states, depends on the natural width of the state under study, defined as $\Gamma = h/(2\pi\tau)$, where τ is the lifetime of the particle, and/or on the experimentally achievable mass resolution. The observed width of particles such as J/ψ or Υ is dominated by the instrumental resolution, whilst that of the Z is dominated by its natural width. The background can also be seen and the clarity (high signal over background) of the signals is evident. The widths of these states are found to be consistent with the design goal, e.g. 0.6% at the Υ mass.

The electromagnetic energy resolution for photons and electrons varies as a function of pseudorapidity due to the differing amount of material traversed. An estimate of the resolution has been made by examining photons that enter the analysis of Higgs bosons decaying into di-photons. These photons lie predominantly in the barrel region and their energy resolution is estimated to be ~1% in the relevant range of energies ($p_T = 25$–100 GeV).

The measurement of the mass of the top quark in lepton+jets final state is illustrative of the global performance of the CMS detector as a whole. Entering this measurement are jet energy resolution, missing transverse energy resolution and the b-tagging capability. For each event the mass is reconstructed from a kinematic fit of the decay products to a $t\bar{t}$ hypothesis. Events are selected with a single isolated lepton ($p_T > 33$ GeV) with at least four jets ($p_T > 30$ GeV), out of which exactly two that must be b-tagged jets. Fig. 13a shows the reconstructed W-boson mass distribution and Fig. 13b the fitted top-quark mass distribution after the goodness-of-fit (gof) selection and the weighting by the P_{gof}. The most precise measurement of the mass of the top quark so far made yields a mass of 172.22 ± 0.73 GeV. The W-boson mass resolution

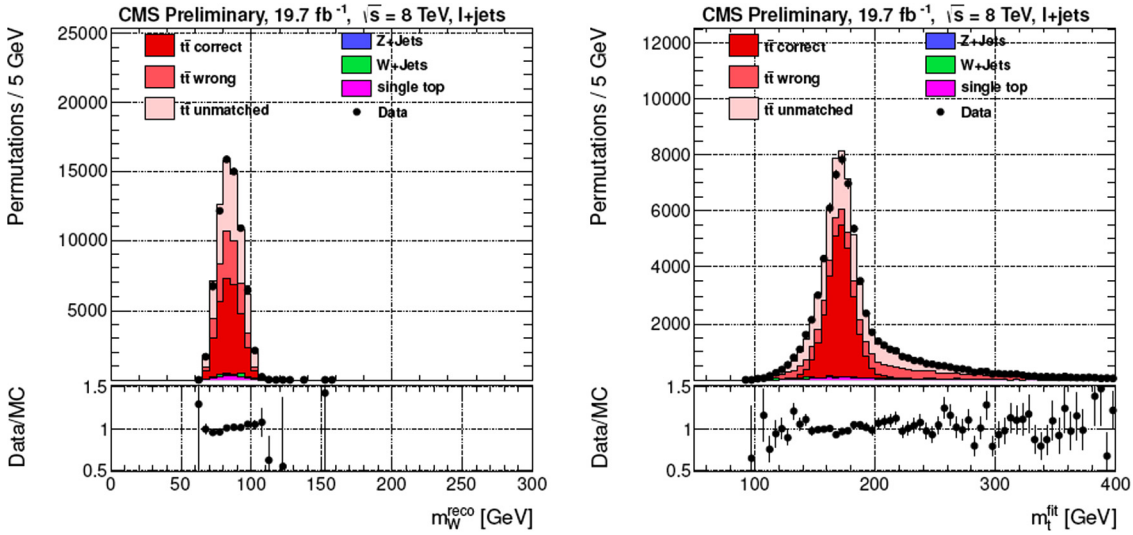

Fig. 13. (Color online.) For the selected events, the mass distributions are shown for (left) the reconstructed W-boson and (right) the top-quark.

is measured to be 12(8.5) GeV for resolved (boosted) jets. The b-tagging efficiency is $\simeq$70% for a fake rate of $\simeq$1.5% for light quarks.

4. Conclusion

The observation of a Higgs boson around 125.5 GeV by ATLAS [3] and CMS [4] in 2012 demonstrated that the two detector designs, rather complementary, are both successful.

References

[1] ATLAS Collaboration, The ATLAS experiment at the CERN Large Hadron Collider, J. Instrum. 3 (2008) S08003.
[2] CMS Collaboration, The CMS experiment at the CERN Large Hadron Collider, J. Instrum. 3 (2008) S08004.
[3] ATLAS Collaboration, Observation of a new particle in the search for the standard model Higgs boson with the ATLAS detector at the LHC, Phys. Lett. B 716 (2012) 1, arXiv:1207.7214.
[4] CMS Collaboration, Observation of a new boson at a mass of 125 GeV with the CMS experiment at the LHC, Phys. Lett. B 716 (2012) 30, arXiv:1207.7235.